Submitted to Ap. J. Letters

Using the High Resolution X-ray Spectrum of PSR B0656+14 to Constrain the Chemical Composition of the Neutron Star Atmosphere

Herman L. Marshall and Norbert S. Schulz

Center for Space Research, MIT, Cambridge, MA 02139

ABSTRACT

Observations of PSR B0656+14 using the Chandra Low Energy Transmission Grating Spectrometer are presented. The zeroth order events are pulsed at an amplitude of 10 ± 2% and the image may be slightly extended. The extended emission is modelled as a Gaussian with a FWHM of about 0.75″, for a linear size (at a distance of 760 pc) of 8.5 $\times 10^{15}$ cm. In the absence of systematic errors in the detector point spread function, the extended emission comprises $\lesssim 50\%$ of the observed flux in the 0.2-2.0 keV band, for a luminosity of $\lesssim 3 \times 10^{32}$ erg s^{-1}. The spectrum is well modelled by a dominant blackbody with $T = 8.0 \pm 0.3 \times 10^5$ K and a size of 22.5 ± 2.1 km in addition to a harder component that is modelled as a hotter and much smaller blackbody. No significant absorption features are found in the spectrum that might be expected from ionization edges of H or He or bound-bound transitions of Fe in magnetized atmospheres. Such features are expected to be deep but could vary in position or strength with rotation phase. There are no strong absorption features in the pulse-phased spectra, however, so we conclude that the atmosphere is not dominated by Fe or other heavy elements that would be partially ionized at a temperature of 10^6K.

Subject headings: stars:neutron — pulsars: individual (PSR B0656+14)

1. Introduction

The X-ray spectra of many "middle-aged" and isolated neutron stars are dominated by a thermal component, so, besides temperatures and radii, they can in principle be used to measure the atmospheric composition. See Becker & Trümper (1997) for a summary

of ROSAT observations of several neutron stars whose X-ray emission could be fitted to blackbody spectra. The composition can, in turn, affect the estimated temperature and size of the emission region (Rajagopal & Romani 1996; Rutledge et al. 1999) but ROSAT spectra were insufficient to determine if there were spectral features that might be expected if cyclotron lines or heavy elements dominate the atmosphere. For example, Rajagopal et al. (1997) showed that an iron-dominated atmosphere in a magnetic field as strong as 10^{12} G would show many narrow absorption features due to the distortion of the energy levels.

PSR B0656+14 is an isolated radio pulsar with a period of about 384 ms, found in the *Einstein* ultrasoft X-ray survey by Cordova et al. (1989). ROSAT observations showed weak pulsations with an amplitude of $\sim 14\%$ (Finley et al. 1992) and that the X-ray spectrum appeared to be well fit with a simple black body model with $T = 9 \times 10^5$ K. From longer ROSAT observations, Possenti et al. (1996) found that the spectrum appeared slightly more complex and that the pulse shape changes with energy. Possenti et al. (1996) fitted a two component model to the pulse light curve and X-ray spectrum, suggesting that the hotter component is emission from the poles and the cooler part comes from the equator but the hotter component could instead be modelled by a steep power law component with $\alpha = 3.5 \pm 0.4$ (where $f_\nu \propto \nu^{-\alpha}$). Edelstein et al. (2000) found a somewhat lower temperature by combining *EUVE*, *ROSAT*, and optical data. Greiveldinger et al. (1996) required two black body components as well as a hard power law ($\alpha = 1.5 \pm 1.1$) to describe the *ASCA* spectra extending to 5 keV. The distance estimated from the pulsar's dispersion measure is 760 pc (Taylor, Manchester, & Lyne 1993).

We observed PSR B0656+14 using the Chandra Low Energy Grating Spectrometer (LETGS) in order to detect narrow X-ray lines in absorption that might be observed if the atmosphere is dominated by iron. The energies of these absorption features should depend on the average magnetic field strength, so we used the High Resolution Camera Spectroscopy (HRC-S) detector which provide event timing to better than 10 μs in order to obtain pulse phased spectra. We find no strong spectral lines and show that the LETGS data are consistent with the previous results; the continuum is well fit by a model involving two black body components. Pulse phased spectra are used to search for spectral features that might be phase dependent.

2. Observations and Data Reduction

2.1. Imaging

PSR B0656+14 was observed with the LETGS on 28 November 1999 (JD - 2451000. = 510.99 - 511.43). The level 0 were processed with CIAO version 2.0b.[1] The exposure time was 38167 s. The count rate in zeroth order was consistent with 0.19 count/s for the entire observation. The bandpass for the zeroth order image is hard to define due to the low energy resolution of the HRC-S, so we estimated the energy range over which one may integrate the spectrum-weighted effective area to obtain 90% of the observed count rate: 0.20 - 0.75 keV. To obtain 99% of the total count rate, the bandpass should be extended to 0.16-1.0 keV. The resultant image was azimuthally symmetric, as expected for a point source.

We tested the radial distribution of events against that of a comparable LETG/HRC-S observation of a point source: Capella (observation ID 1248). Due to the dispersion by the fine and coarse support structure, the point response function of the LETGS zeroth order image depends slightly on the spectrum of the source. The zeroth order image yielded 180440 events within $5'$ of the centroid in 85260 s. The spectrum of Capella is soft but is harder than that of the pulsar, so we divided the data into two equal parts based on the pulse height distribution. The average pulse height for the low half is quite similar to that of PSR B0656+14, but the radial profile differs by no more than 1.5% from the average profile using all events so we used the average profile for comparison to the pulsar. The encircled power was modelled as the sum of Gaussian and exponential components, representing the Capella data to better than 1.5% over the 0-5″ range:

$$\Phi(\theta) = (1-f)[1-e^{-\theta^2/\sigma_{PSF}^2/2}] + f[1-e^{\theta/\theta_0}], \quad (1)$$

where θ is the angle from the centroid, $f = 0.31$ is the fraction of the power in the exponential component, σ_{PSF} is the Gaussian width parameter of the point spread function (PSF), and θ_0 is the scaling length of the exponential component. Capella is very bright, so the background has a negligible contribution ($< 1\%$) to the radial profile out to 5″ from the source centroid. For the pulsar, background was estimated from an annulus 8-10″ from the source centroid.

The cumulative event radial profiles are given in Fig. 1. The profiles are normalized to unity at 5″. The pulsar's radial distribution differs from Capella's by $\sim 8.5\%$ at 0.5″, indicating that the X-ray source may consist of a point source and some distributed emission

[1]CIAO is the Chandra Interactive Analysis of Observations, a software system developed by the Chandra X-ray Center.

that is extended on a scale of order 0.5″. A Smirnov test indicates that a 5% difference between the Capella and PSR B0656+14 profiles would be significant at the $> 8\sigma$ level and that differences of 1.6% are significant at the 2σ level. We modelled the profile by combining a Gaussian model of the extended emission with a PSF model. The model of the extended emission was constructed using the PSF model but increasing the Gaussian width parameter by combining a second term in quadrature, σ_{ext}. The model for the pulsar's radial distribution is matched to about 2% when $\sigma_{ext} = 0.32''$ and the extended component comprises 50% of the total power. The uncertainties are difficult to characterize and are probably dominated by systematic uncertainties in the PSF. Given the possible systematic uncertainties in these early HRC-S imaging data, we estimate that an unresolved source accounts for $\gtrsim$ 50% of the profile and that the FWHM of the extended emission is in the range of 0.2-0.5″.

2.2. Timing

The zeroth order image was used to determine the phase and period of the X-ray pulsations. After applying timing corrections to the solar system barycenter and correcting for the satellite's position in orbit, we determined that the pulse period was 384.8990 ms with a 1 σ uncertainty of 0.0010 ms using a χ^2 test on folded light curves. This period is consistent with the predicted value, 384.89970 ms from radio pulse monitoring (Andrew Lyne, 2001, priv. communication). The pulse light curve shown in Fig. 2 was folded using the radio ephemeris. The pulse appears to be asymmetric, as previously found by Possenti et al. (1996). The modulation amplitude is 10 ± 2%, defined as $(R_{max} - R_{min})/(R_{max} + R_{min})$, where R_{max} and R_{min} are the maximum and minimum of the pulse light curve, respectively. This value is consistent with the pulse fractions obtained by Finley et al. (1992) (14 ± 2%) and Possenti et al. (1996) (9 ± 1%).

The radio phase is defined so that the peak of the radio pulse occurs at a phase of zero. Fig. 2 shows that the X-ray peak is at about phase 0.85, which is about 55° out of phase with the radio phase. The absolute timing HRC-S has been verified to an accuracy of $<$ 0.001 s using the Crab pulsar (Allyn Tennant, 2001, priv. comm.).

2.3. Spectroscopic Data Reduction

The spectral data were reduced from standard event lists using IDL using custom processing scripts; the method is quite similar to standard processing using CIAO. The proce-

dure was to: 1) select data based on the criteria suggested by the Chandra X-ray Center (CXC) LETGS calibration team[2] in order to reduce background, 2) determine the location of zeroth order using one dimensional profiles fitted to Gaussians, 3) rotate events from sky coordinates to compensate for the telescope roll and correct for a 0.54″ offset between HRC-S plates 0 and 1, 4) compute the dispersed grating coordinates ($m\lambda$ and θ) using the grating dispersion angles and the dispersion relation, 5) select "source" events spatially within oppositely curving parabolas of the dispersion line as suggested by the CXC LETG calibration team [3], 6) eliminate data affected by detector gaps, and 7) bin events at $\Delta\lambda$ =0.025Å.

The effective area (EA) of the LETGS has undergone a few revisions since launch both due to a recalculation of the LETG efficiencies and due to a long series of in-flight calibration observations designed to probe the HRC-S quantum efficiency. We started with the updated LETGS EA that was released by the CXC of 31 October 2000[4]. These LETG efficiencies were used, along with the transmission models of the UV ion shield, to determine the effective areas for orders 2 through 5. In a final step, an adjustment to the pre-flight calibration was applied which was derived from an analysis of the spectrum of Mrk 478 (Marshall et al. 2002) and PKS 2155-304 (Marshall et al. 2002, in preparation). The spectra of both targets are well fit by a simple power law with Galactic absorption. The adjustments affect primarily the spectrum at low energies ($E < 0.2$ keV), where high order contributions are beginning to be important.

Directly totalling the observed fluxes over the 0.2-3.0 keV band gives an observed flux of 1.01 $\pm 0.03 \times 10^{-11}$ erg cm^{-2} s^{-1} for an absorbed luminosity of 7.0 $\pm 0.2 \times 10^{32}$ erg s^{-1}. The data were rebinned adaptively to provide a signal/noise ratio of 5 in each bin over the 0.10 to 2.0 keV range. The spectrum, shown in Fig. 3, was estimated using the first order EA only. The contributions to the observed counts due to high orders are estimated by folding a model for first order through the high order EA and dividing by the first order EA. This procedure has the disadvantage that all the spectral features in the high order EAs are apparent but the advantage is that the result will match the intrinsic spectrum well if first order dominates. For this source, high orders are negligible above 0.20 keV.

---

[2]Chandra calibration information is available at the CXC web site:`http://cxc.harvard.edu/cal/`. The HRC-S selection recommendation can be found at: `http://cxc.harvard.edu/cal/Links/Letg/User/Hrc_bg/`.

[3]See `http://cxc.harvard.edu/cal/Links/Letg/User/Hrc_QE/EA/Wads`.

[4]This effective area is available at `http://cxc.harvard.edu/cal/Links/Letg/User/Hrc_QE/EA/correct_ea/letgs_NOGAP_EA_001031.mod`.

3. Modelling the Spectrum

Following previous analyses, we modelled the continuum with two blackbody components. Our objective is primarily to define a smooth continuum model to use as a baseline for line searches. We did not include the hard power law component found by Greiveldinger et al. (1996) because its contribution in the 0.2-1.0 keV band is negligible. We exclude the data below 0.15 keV from the fit where uncertainties in the high order grating efficiencies can be important. Gaussian statistics could be used for continuum modelling by rebinning to obtain a signal/noise ratio of at least 5 in each bin, giving reduced $\chi^2 = 1.13$, acceptable at the 90% level. The distribution of the residuals is not consistent with a Gaussian, however; the Kolmogorov test rejects at the 99.99% confidence level due to systematic skewing of the residuals to positive values. This may result from systematic errors at the 5-10% level in the 0.45-0.55 keV portion of the spectrum.

The best fit temperatures of the two blackbody components were $8.0 \pm 0.3 \times 10^5$ and $1.6 \pm 0.3 \times 10^6$ K and the radii were 22.5 ± 2.1 and 1.7 ± 1.0 km, respectively. The best-fit interstellar medium (ISM) column density, N_H, was $1.73 \pm 0.18 \times 10^{20}$ cm^{-2}. These parameters are close to those found by Greiveldinger et al. (1996). The best fit model is plotted against the fitted data in Fig. 3. The count spectrum (Fig. 4) was binned at 0.125 Å resolution in order to search for narrow spectral features against the continuum model. No significant absorption features were found. A fit to a nonmagnetized H atmosphere (Zavlin, Pavlov, & Shibanov 1996) gave a much lower temperature, 230000 K, a very large radius, 413 ± 53 km and a much larger N_H, $2.6 \pm 0.2 \times 10^{20}$ cm^{-2}.

The data were divided into pulse maximum and minimum by phase: 0.05-0.55 and 0.55-1.05 (see Fig. 2). The difference spectrum (Fig. 5) shows a dip in the 45-50 Å region. The pulse amplitude spectrum was defined as the ratio of the difference spectrum to the model of the pulse-averaged spectrum and is also shown in Fig. 5. The result is rather flat, consistent with being constant over this wavelength band.

4. Discussion and Summary

Models of a neutron star atmosphere dominated by Fe in a strong magnetic field, such as computed by Rajagopal et al. (1997), should show deep narrow features which we do not observe. For a hydrogen atmosphere, however, there are very few spectral features but the radius of the fitted nonmagnetized H atmosphere is much too large. In order to reduce the apparent radius to 13 km (appropriate for a neutron star with a mass of 1.4 $M_\odot$ and a radius of 10 km), the distance would have to be absurdly small – 24 pc – given the large N_H and the

large distance from the dispersion measure. For the blackbody model, however, the distance would have to be about 440 pc, which is consistent with the estimate from the pulsar's dispersion measure. For a magnetized H atmosphere, results are similar to the case with $B = 0$ but are not quite so extreme. Meyer et al. (1994) found that the *ROSAT* spectrum of Geminga fit a blackbody with $T = 7.6 \times 10^5$ K while a magnetized H atmosphere gave $T = 5.0 \times 10^5$ K for $B = 4.7 \times 10^{12}$ G. The magnetic field estimated for PSR B0656+14 is the same (Taylor, Manchester, & Lyne 1993), so one might expect a similar reduction when fitting the PSR B0656+14 spectrum. In order to generate the same observed flux, the radius of the emission region would have to increase by a factor of 2.3 to 52 ± 5 km so the distance would have to be reduced to 190 pc. A distance to less than 200 pc can be definitely ruled out using the dispersion measure and a more refined model of the local ISM (J. Cordes, 2002, private communication).

We find no significant absorption features in the pulse-averaged or pulse-phased spectra over the 0.15-0.80 keV band. Thus, we can rule out electron and proton cyclotron resonance lines, which should be rather deep and possibly broadened, according to models by Zane et al. (2001) and Ho & Lai (2001). The proton cyclotron line would be expected at an observed energy $E_o = E_p/(1+z) = \hbar eB/(m_p c)/(1+z) = 0.0063/(1+z)B_{12}$ keV, where $B_{12} = B/(10^{12}$ G) and $z = (1 - 2GM/Rc^2)^{-1/2} - 1$ is the surface redshift. Substituting the electron mass for the proton mass, m_p, gives the electron cyclotron line energy $E_e/(1+z) = \hbar eB/(m_e c)/(1+z) = 1.16/(1+z)B_{12}$ keV. Thus, we eliminate the ranges $0.017 < B_{12} < 0.090$ and $30 < B_{12} < 165$ if $z = 0.30$ (for a neutron star of 1.4 $M_\odot$ and a radius of 10 km). These ranges do not exclude the magnetic field estimate from the dipole braking model: $B_{12} = 4.7$ (Taylor, Manchester, & Lyne 1993). The lower limits can be reduced if the bulk of the emission comes from the equatorial zone where the magnetic field is $\sim 50\%$ of the polar value or if the absorbing plasma is far off of the neutron surface.

For this dipole field estimate, a light element atmosphere should show H or He ionization edges in the 0.15-0.80 keV bandpass. Lai & Salpeter (1997) give an estimate for the ionization edge energy and its dependence on the atomic number Z:

$$E_Z = 4.4 Z^2 [\ln(\frac{B}{Z^2 B_0})]^2 \ \text{eV} \tag{2}$$

where $B_0 = 2.35 \times 10^9$ G. A He I edge would be expected in the 0.5-0.7 keV range. We do not detect this edge, which may not be surprising, as helium may have settled in the atmosphere to high optical depths. For surface temperatures of 9-22 $\times 10^5$ K (allowing for variation between the pole and the equator), He is almost completely neutral while H is 7-22% ionized. So, we expect to find the H I edge between 0.20 and 0.25 keV (depending on the surface gravity) but it is not observed. The spectrum is dominated by the cooler thermal

component, however, which is presumably emission from the equatorial zone in which B is $\sim 2\times$ weaker than at the pole. Thus, the edge may be found in the 0.16-0.21 keV region, where the signal/noise ratio is poor and high order contributions to the LETGS spectrum become important.

Most of a pulsar's spin-down luminosity is thought to be carried off as a relativistic electron/positron wind. When this wind is confined by external pressure, a shock forms and the relativistic particles radiate synchrotron emission in the form of a pulsar wind nebula (PWN). The Crab Nebula (Hester et al. 1995, Weisskopf et al. 2000) is the best known example. PWNe have been observed around at least 6 pulsars so far (Becker & Trümper 1997; Lu et al. 1997). Claims from ASCA observations of vastly extended PWNe ($>$ 10-20$'$) in this and other pulsars with luminosities of the order of 10^{32} erg s^{-1} have not been confirmed by *ROSAT* and *BeppoSAX* (Becker et al. 1999). We also do not detect such a large extended nebula around PSR B0656+14. The image appears slightly extended, consistent with a point source comprising $\gtrsim 50\%$ of the total 0.1-3 keV luminosity. The remainder, with an unabsorbed luminosity of $\lesssim 3\times10^{32}$ erg s^{-1} can be modelled with a Gaussian with a FWHM of 0.75$''$ corresponding to a size of 8.5 $\times10^{15}$ cm. This extended emission is consistent with the result of Becker et al. (1999), who found that a PWN around PSR B0656+14 must have an extent of less than 10$''$. Based on its spin-down age, $\sim 10^5$ yr, PSR B0656+14 is an order of magnitude older than the Vela pulsar, the oldest pulsar around which a PWN has been detected (Becker & Trümper 1997). If we assume a similar emission efficiency for PSR B0656+14 as for the Vela pular ($\sim 0.04\%$), we can set an upper limit to the expected luminosity of the PWN of 1.5×10^{33} erg s^{-1}, consistent with the observed value.

We are extremely grateful to Prof. Claude R. Canizares, the Principal Investigator of the *Chandra* High Energy Transmission Grating Spectrometer, for allocating part of his guaranteed time to this observation. We thank the referee for comments that have resulted in significant improvements to the paper. This work has been supported in part under NASA contract SAO SV1-61010.

REFERENCES

Becker, W., & Trumper, J., 1997, A&A, 326, 682

Becker, W., Kawai, N., Brinkmann, W., and Mignani, R. 1999, A&A, 352, 532

Cordova, F.A., Hjellming, R.M., Mason, K.O., and Middleditch, J., 1989, ApJ, 345, 451

Edelstein, J., Seon, K.-I., Golden, A., and Min, K.-W. 2000, ApJ, 539, 902

Finley, J., Ögelman, H. & Ziziloğlu, Ü. 1992, ApJ, 394, L21

Greiveldinger, C., et al. 1996, ApJ, 465, L35

Hester, J.J., et al. 1995, ApJ, 448, 240

Ho, W., & Lai, D. 2001, MNRAS, 327, 108

Lai, D., & Salpeter, E.E. 1997, ApJ, 491, 270

Lu, F.J., Wang, Q.D., Aschenbach, B., Durouchoux, P., Song, L.M. 2002, ApJ, in press

Marshall, H.L., Edelson, R.A., Vaughan, S., Warwick, R., Malkan, M., and O'Brien, P. 2002, ApJ, submitted

Meyer, R.D., Pavlov, G.G., and Meszaros, P. 1994, ApJ, 433, 265

Rutledge, R. E., Bildsten, L., Brown, E. F., Pavlov, G. G., & Zavlin, V. E. 1999, ApJ, 514, 945

Pavlov, G.G., Welty, A.D., and Cordova, F.A. 1997, ApJ, 489, 75

Possenti, A., Mereghetti, S., and Colpi, M. 1996, A&A, 313, 565

Rajagopal, M., & Romani, R.W., 1996, ApJ, 461, 327

Rajagopal, M., Romani, R.W., and Miller, M.C. 1997, ApJ, 479, 347

Taylor, J. H., Manchester, R. N., & Lyne, A. G. 1993, ApJS, 88, 529

Tsuruta, S., 1998, Phys. Rep., 292, 1.

Weisskopf M.C., et al., 2000, ApJ, 536, L81

Zane, S., Turolla, R., Stella, L. & Treves, A. 2001 ApJ, 560, 384

Zavlin, V. E., Pavlov, G. G., & Shibanov, Y. A. 1996 A&A, 315, 141

AAS LaTeX macros v5.0.

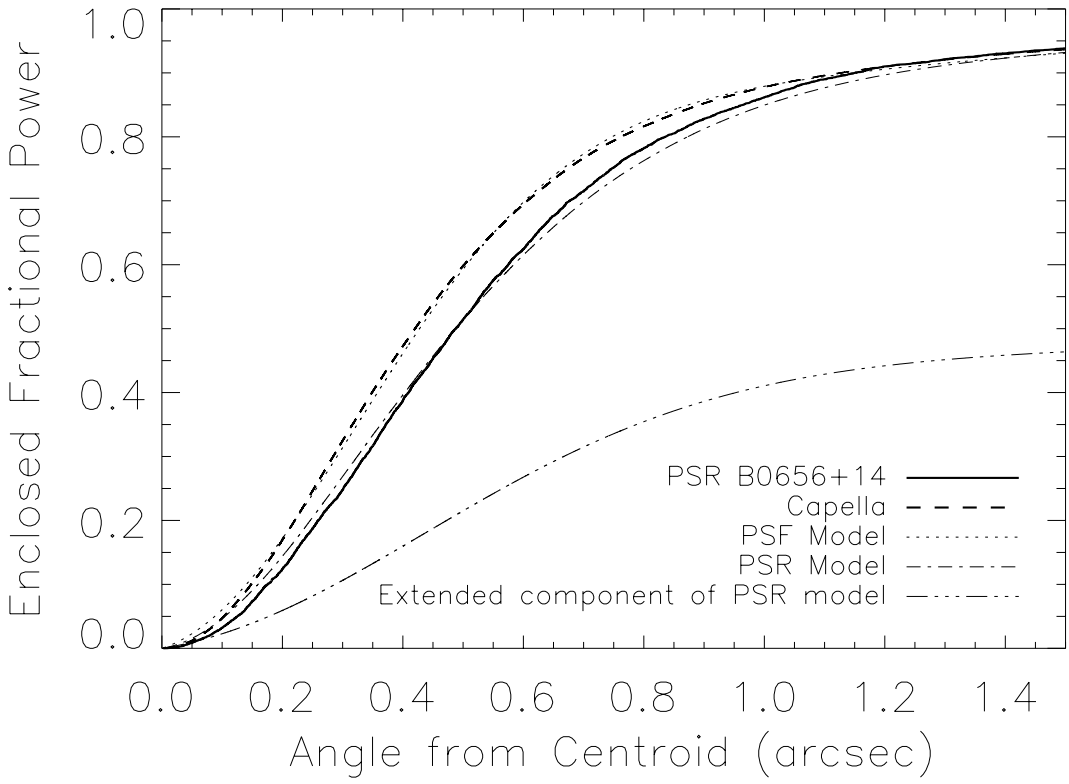

Fig. 1.— Enclosed fractional power for the pulsar, PSR B0656+14 (solid line), and for Capella (dashed line). The pulsar's profile is somewhat broader than that of Capella, giving an indication that there is some extended emission around the neutron star. A model of the point spread function (PSF) was fitted to the Capella data. The model of the pulsar's power profile consists of a PSF and an extended emission modelled by a Gaussian with $\sigma_{ext} = 0.32''$ convolved with the PSF. All profiles (except the extended component) are normalized to unity at an angle of $5''$ from the image centroid. Given the possible systematic uncertainties in early HRC-S data, we estimate that a point source contributes $\gtrsim 50\%$ of the source flux.

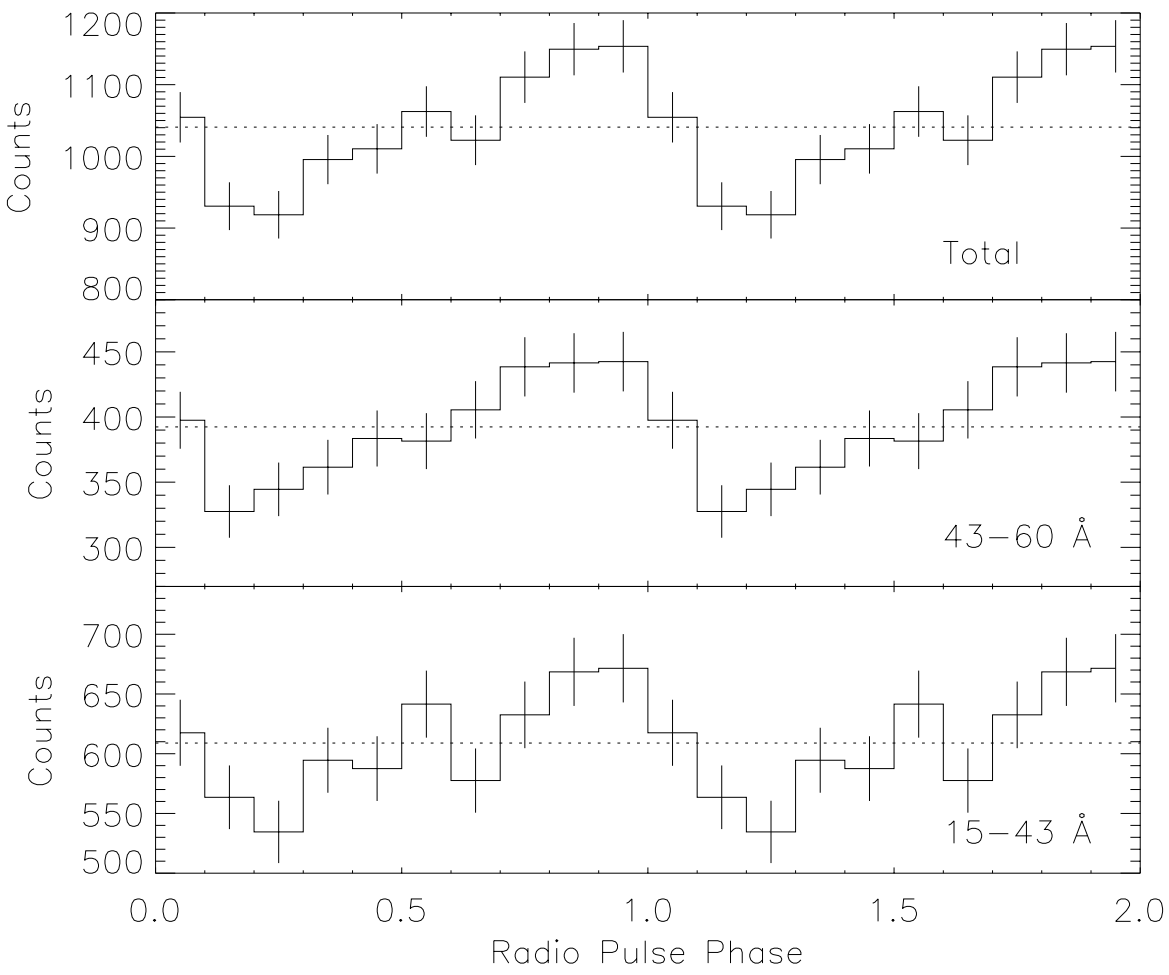

Fig. 2.— The pulse profile of the zeroth order events. *Bottom:* Hard bandpass (15-43 Å, or 0.29-0.83 keV), *middle:* soft bandpass (43-60 Å or 0.21-0.29 keV), *top:* total (15-60 Å or 0.21-0.83 keV). The data are replicated to the phase range 1-2 for presentation. An unpulsed background level was subtracted from each profile. The events are folded at the period given by an accurate radio pulse ephemeris (Andrew Lyne, private communication): 384.89970 ms. The pulse is asymmetric and the peak is centered at phase 0.85 where zero phase is defined to be the peak of the radio pulse. Thus, it appears that the X-ray pulse somewhat leads the radio pulse by about 0.15 in phase. The soft and hard pulse profiles are quite similar.

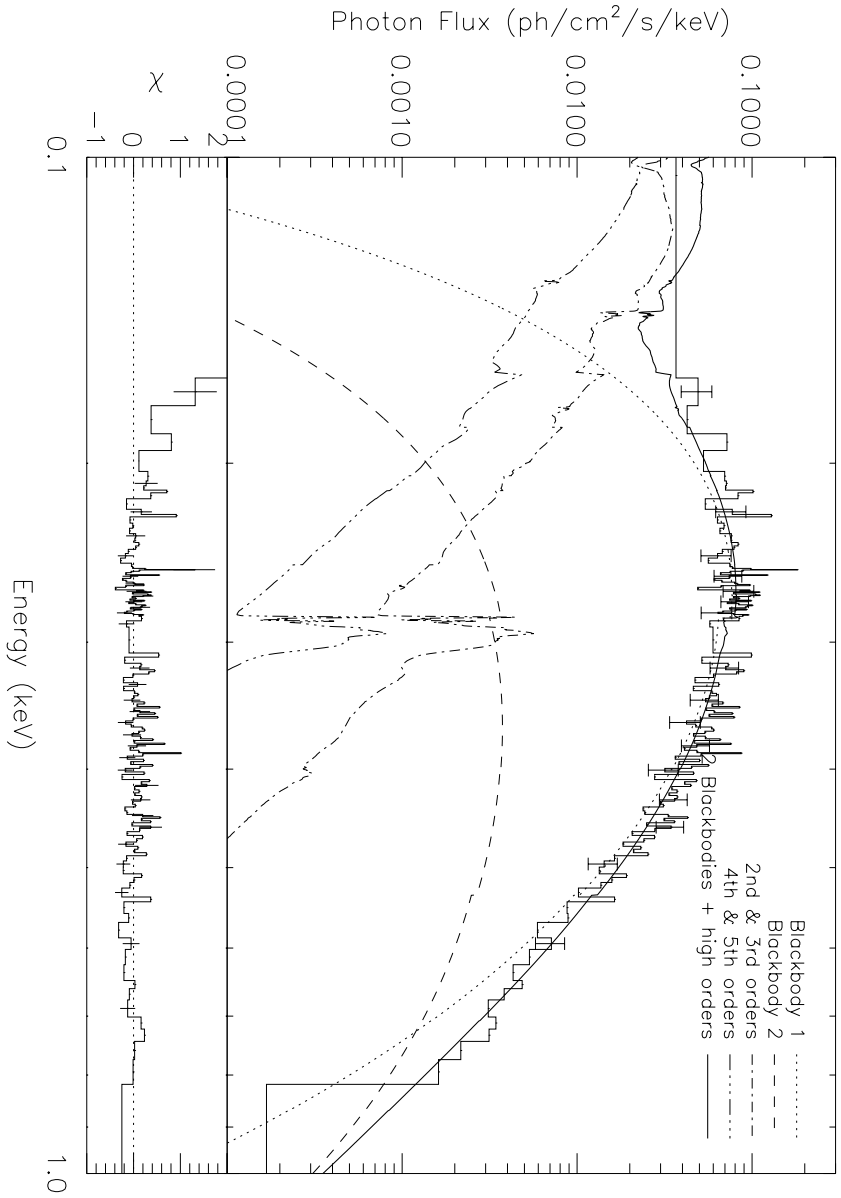

Fig. 3.— The LETGS spectrum of PSR B0656+14. The bin sizes have been varied to provide good signal in each energy bin; the uncertainties are about 20% everywhere. *solid line:* a model consisting of two blackbody components. The lower panel shows the residuals as ratios to the uncertainties. High orders do not contribute significantly for $E > 0.20$ keV while the data at low energies ($E < 0.15$ keV) are best modelled as the result of the sum of high orders. The cooler blackbody component dominates the total power while the hotter component dominates the spectrum for $E > 0.8$ keV.

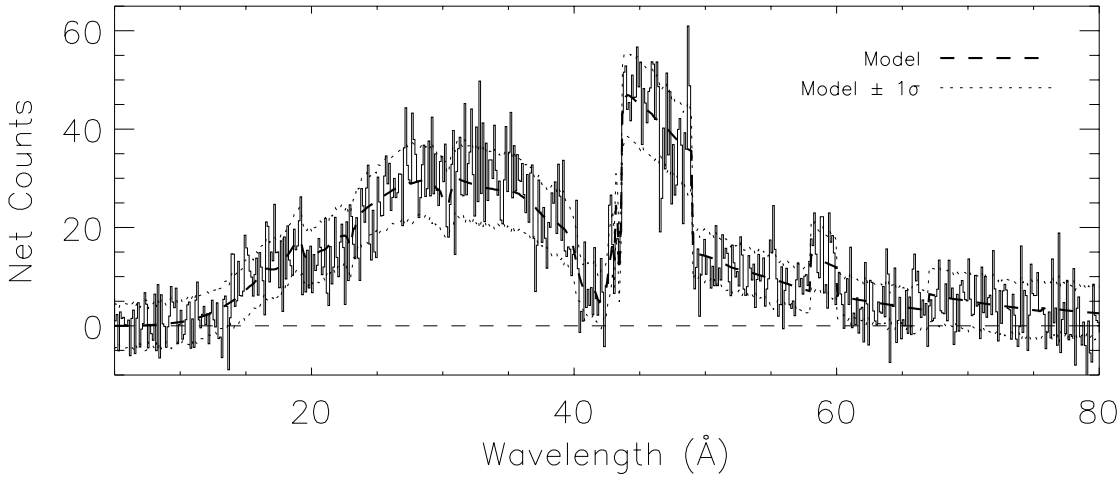

Fig. 4.— The count spectrum of PSR B0656+14 obtained with the LETGS. A binning of 0.125Å was used to obtain sufficient signal per bin to search for narrow features. *Heavy dashed line:* expected count spectrum from the model shown in figure 3. *Light dotted lines:* ± 1 σ uncertainties about the model. The residuals are consistent with statistical fluctuations about the model. The sharp edges in the model near 50 to 70Å range are due to detector gaps.

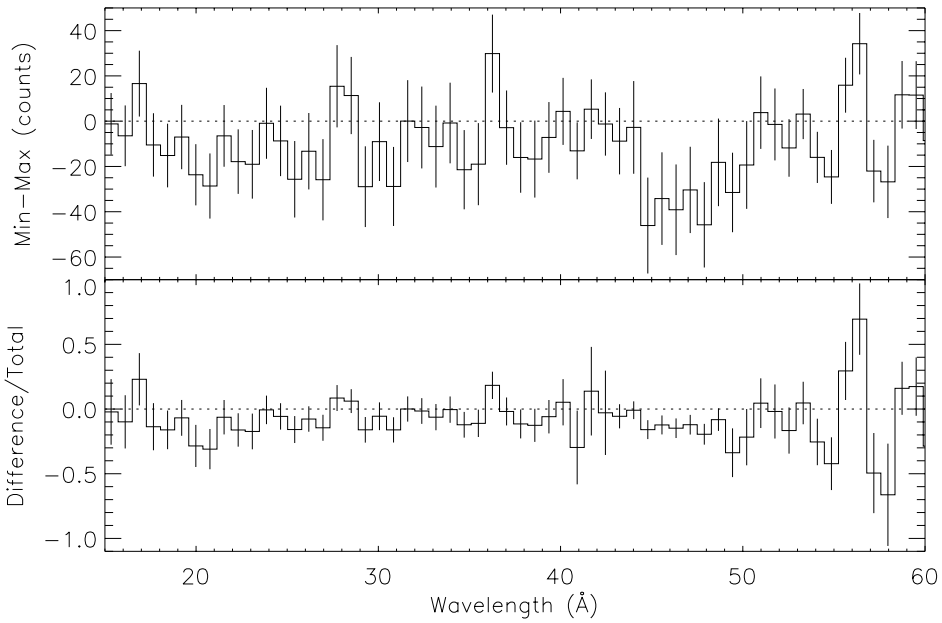

Fig. 5.— Difference spectra in 0.775Å bins. The spectrum from the phase range 0.55-1.05 (see Fig. 2) is subtracted from the remaining phase range. In the bottom panel, the difference spectrum is divided by the model of the total spectrum, giving a fractional residual. In the 45-50Å band, there is a dip in the minimum spectrum relative to that of pulse maximum, which is clearly detected in the count spectrum. The bottom panel shows that the residuals are generally consistent with a $\sim 8\%$ difference between the two spectra that is independent of wavelength.